Journal of Hazardous Materials 209–210 (2012) 385–391

Contents lists available at SciVerse ScienceDirect

Journal of Hazardous Materials

journal homepage: www.elsevier.com/locate/jhazmat

Shape-controlled fabrication of the porous Co_3O_4 nanoflower clusters for efficient catalytic oxidation of gaseous toluene

Qingyun Yan[a], Xinyong Li[a,b,*], Qidong Zhao[a], Guohua Chen[b]

[a] Key Laboratory of Industrial Ecology and Environmental Engineering (MOE), State Key Laboratory of Fine Chemical, School of Environmental Science and Technology, Dalian University of Technology, Dalian 116024, China

[b] Department of Chemical and Biomolecular Engineering, The Hong Kong University of Science and Technology, Clear Water Bay, Kowloon, Hong Kong

ARTICLE INFO

Article history:
Received 1 November 2011
Received in revised form 11 January 2012
Accepted 13 January 2012
Available online 20 January 2012

Keywords:
Low-temperature hydrothermal method
Co_3O_4 nanoflower clusters
Toluene
Catalytic oxidation

ABSTRACT

Co_3O_4 nanoflower clusters were fabricated by a simple low-temperature hydrothermal method. The properties of Co_3O_4 nanomaterials were comprehensively determined by combining different analytical techniques. The self-assembled Co_3O_4 nanoflower clusters had good crystallinity and porous structure. They were utilized as the catalyst for the degradation of gaseous toluene. The experimental results showed that the catalytic activity of the as-prepared Co_3O_4 nanoflower clusters was much superior to the Co_3O_4 blocks under the same reaction conditions.

.

1. Introduction

There are many techniques to remove the volatile organic compounds (VOCs), which are common air pollutants to human health. These techniques include adsorption, catalytic combustion, photocatalytic degradation and physical separation. For example, Everaert et al. [1] have utilized membrane separation techniques for the separation of gases and vapors. Among the techniques, catalytic combustion of VOCs is always a hot topic investigated by many researchers. Among various VOCs, toluene is a typical gaseous pollutant difficult to remove at moderate temperature due to its chemical stability. Everaert et al. [2] studied the $V_2O_5/TiO_2/WO_3$ catalyst for removing various VOCs. They suggested chlorinated aromatics are easier to oxidize than the pure aromatics with $V_2O_5/TiO_2/WO_3$ as catalyst.

Noble metal based catalysts are traditionally used in VOCs catalytic degradation, but they are too expensive for daily use. Transition metal oxides are an important category of catalysts in many catalytic reactions and they have served as the substitute for the transitional noble catalysts. Transitional metal oxides have been demonstrated to be active and cost effective in VOCs removal as alternatives to noble metals. It has been found that such kinds of catalysts can reduce the activation energy for the catalytic oxidation [2]. Meanwhile, there is a growing potential to promote their activity with the advance in nanotechnology. It is very attractive to investigate the nanostructured transitional metal oxides for enhanced VOCs removal performance.

Co_3O_4 is a p-type magnetic semiconductor with the normal spinel structure, where O^{2-} is cubic close packed, Co^{2+} is in a tetrahedral coordination and Co^{3+} is in an octahedral coordination. The lowest Co—O bonds strength and the highest capability of the activation of molecule oxygen play crucial roles in the catalytic oxidation systems [3]. Due to its special physical and chemical properties, Co_3O_4 is widely used in magnetism [4], photovoltaics [5,6], chemical sensors [7], homogeneous catalysis [8].

Because the structure (microstructure), size, and morphology significantly influence the material properties and application, controlling the morphology of inorganic nanomaterials through proper synthetic strategy plays a central role in obtaining nanomaterials with novel properties. The morphology of Co_3O_4 based nanomaterials is diverse and experimentally available owing to the special spinel structure. The researchers have synthesized hollow nanospheres [9,10], octahedrons [11,12], nanorods [13,14], nanosheets [15,16] as well as hollow sphere clusters [17] and arrays [18] by assembling these units. Nevertheless, it is still a hot theme to fabricate the Co_3O_4 nanomaterials with different morphologies in order to promote the performance [19–22].

* Corresponding author at: Key Laboratory of Industrial Ecology and Environmental Engineering (MOE) and State Key Laboratory of Fine Chemical, School of Environmental Science and Technology, Dalian University of Technology, Dalian 116024, China. Tel.: +86 411 8470 7733; fax: +86 411 8470 7733
E-mail address: xyli@dlut.edu.cn (X. Li).

0304-3894/$ – see front matter © 2012 Elsevier B.V. All rights reserved.
doi:10.1016/j.jhazmat.2012.01.039

Recent reports [22–24] have demonstrated that cobalt oxide is relatively superior to other similar metal oxides in catalytic degradation of toluene. Previous researchers usually used cobalt oxide as the active component loaded on molecular sieves and other supports with large surface area [25]. The large surface area of the supports can make cobalt oxide loading uniform and well dispersed, which not only exposes more cobalt active sites but also increases the contact area between the catalyst and the gaseous toluene. In addition, some researchers prepared composites by combining the cobalt oxide with other metal oxides compound to form bi-metal or multi-metal oxides [26] in order to improve the catalytic activity. This method utilized the synergy between the cobalt oxide and other metal oxides to increase the conversion rate of toluene. However, it has rarely been reported that the catalytic oxidation of toluene could be enhanced just using Co_3O_4 as the single metal oxide catalyst by controlling the particle size and morphology.

In this paper, nanoflower-shaped Co_3O_4 was fabricated by a low-temperature hydrothermal method. The influence of the preparation conditions such as the composition of the precursor (cobalt hydroxycarbonate) on the microstructure of Co_3O_4 sample has been systematically explored. Then, a series of characterization techniques were employed to study the crystal structure, surface properties and the morphologies of the as-prepared Co_3O_4 sample. Finally, the catalytic activity of the as-prepared Co_3O_4 nanoflower clusters for degrading the toxic toluene was further studied by comparing with Co_3O_4 blocks.

2. Experimental

2.1. Preparation of catalysts

Co_3O_4 was prepared by low-temperature hydrothermal method. All chemicals were of analytical grade. In a typical procedure, 2.91 g $Co(NO_3)_2{\cdot}6H_2O$, 0.6 g $CO(NH_2)_2$ and 0.25 g polyvinylpyrrolidone (PVP; MW = 30,000) were added to 100 mL distilled water under stirring for 30 min to form homogeneous solution. The obtained mixture was transferred into the stainless steel autoclaves with a Teflon liner of 120 mL in capacity, which was then heated in an oven at 95 °C for 12 h. After the autoclave was air-cooled to room temperature, the black products were collected and washed with distilled water and absolute ethanol for several times by a centrifugation–redispersion process, followed by drying under vacuum at 60 °C. The as-prepared powder was converted into Co_3O_4 via thermal decomposition at 300 °C for 5 h in air with a ramping rate of 10 °C/min.

2.2. Characterization

The X-ray powder diffraction (XRD) pattern was recorded on a Rigaku D/max X-ray diffractometer (Cu Kα radiation, λ = 0.15418 nm), and the scanning range was 10–70°. The JEOL JSM-6360LV scanning electron microscope (SEM) was used to study the size and morphology of nanomaterials. A small amount of sample was placed in a carbon-coated grid and subjected to the measurements on JEM 2100 transmission electron microscopy (TEM). Hydrogen temperature programmed reduction (H_2-TPR) was carried out in a Quantachrome Chem-BET Pulsar TPR (p/n 02139-1). The band gap of the Co_3O_4 was determined by UV–vis spectroscopy, using a UV-1100 spectrometer. The N_2 adsorption–desorption isotherm was recorded at 77 K using a Quantachrome NOVA instrument. Before the measurement, the sample was degassed at 300 °C for 4 h. The specific surface area was calculated by multipoint Braunauer–Emmett–Teller (BET) analysis of the nitrogen desorption isotherm. The Raman spectrum was taken using a micro-Raman/Photo-luminescence system with 632 nm wavelength laser. Electronic paramagnetic resonance (EPR) experiments were performed with a klystron operating in the X band (ν = 9.5 GHz) as microwaves generator. The data of Fourier transform infrared spectroscopy (FTIR) were recorded on a BRUKER VERTEX 70 spectrometer from 400 to 4000 cm^{-1} at room temperature on KBr mulls. X-ray photoelectron spectra (XPS) data was recorded by a Multilab 2000 electron spectrometer using acrochromatic Al Kα radiation (1486.6 eV).

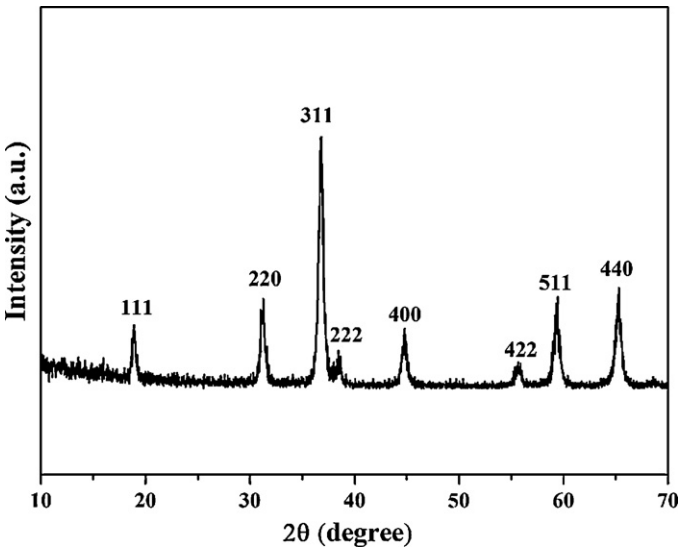

Fig. 1. XRD pattern of the as-prepared Co_3O_4 sample.

2.3. Catalytic oxidation performance

Complete oxidation of toluene was performed in a fixed bed continuous flow quartz micro-reactor under atmospheric pressure using Agilent 7890 A gas chromatograph (GC). 0.2 g (60–80 mesh) catalysts were subjected to tableting, crushing and screening and then put in the reaction tube. Before reaction, the catalysts were pretreated with O_2/Ar (33 mL/min) at 300 °C for 1 h. The reactor space velocity was 37,500 h^{-1}. Ar was employed as the carrier gas at the rate of 50 mL/min to the pure toluene in liquid phase, which was cooled by the ice water bath. The initial concentration of gaseous toluene was about 1000 ppm by detection. The inlet flow was a mixture of Ar with toluene (50 mL/min) and O_2/Ar (33 mL/min). The effluents from the reactor were analyzed with a flame ionization detector (FID) and TCD detector. The temperature range was set at 125–300 °C.

3. Results and discussion

3.1. Catalyst characterization

Fig. 1 shows the XRD pattern of the sample prepared by calcining the cobalt precursor at 300 °C for 5 h. All the diffraction peaks can be indexed as cubic Co_3O_4 with the lattice constant (a = 0.8084 nm), which are consistent with the values in the standard card (JCPDS Card No. 43-1003). Sharp peaks suggest the sample has a good crystallinity of pure Co_3O_4 phase. No peaks from other phases are observed in this pattern.

In the FTIR spectrum of the precursor (Fig. 2), the two peaks at 1500 and 1350 cm^{-1} correspond to the symmetric and asymmetric stretching vibrations of υ (NO_3), respectively. The bands centered at about 829 and 687 cm^{-1} are assigned to the stretching vibrations of δ (CO_3) and ρ (OCO) in the carbonate anion, respectively.

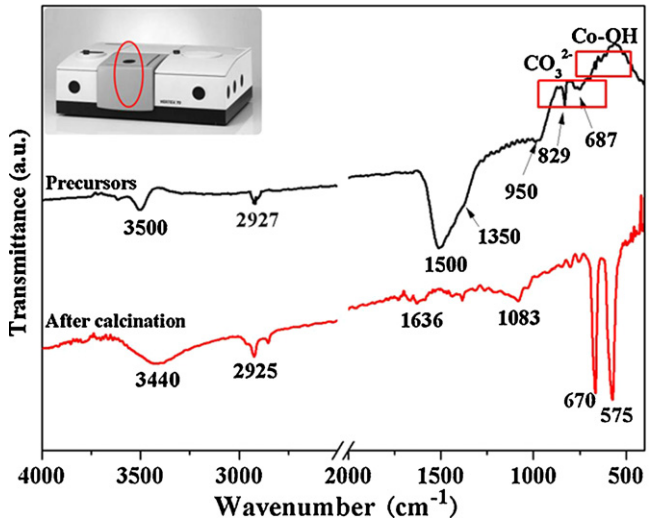

Fig. 2. The FTIR spectra of the precursor before calcination and the as-obtained Co_3O_4 sample.

The peak at about 950 cm^{-1} can be ascribed to the δ (Co—OH) bending vibration, and the unobvious band between 510 and 540 cm^{-1} represents the ω (Co—OH). Therefore, the precursor is definitely nitrate-containing cobalt hydroxycarbonate [27]. In the FTIR spectrum of the sample after calcination, the peaks at 670 and 575 cm^{-1} are the characteristic absorption peaks of Co_3O_4 spinel oxide. For both FTIR curves of the precursor and the calcined sample, the broad band between 3440 and 3500 cm^{-1}, and the peak at 1636 cm^{-1} could be assigned to the O—H stretching and bending modes of water and surface hydroxyl groups. The absorption peaks at 2925, 2927 and 1083 cm^{-1} are assigned to C—H stretching vibrations from PVP [4].

Fig. 3 shows the morphological and structural properties of the as-prepared Co_3O_4 sample. Fig. 3a and d shows the Co_3O_4 nanoflower clusters are assembled by the many nanowires with the diameter of about 20 nm and the length of 3–6 μm. The TEM image in Fig. 3d reveals that there is a large amount of nanoparticles with an average size of several nanometers along the original longitudinal directions of the wires, which may greatly increase their surface area [28] and improve the chemical properties or serve as transport paths for small molecules. The mesoporous Co_3O_4 nanowires are presented in Fig. 4, which shows that the nanowires are closely packed. Closely packed nanowires can constitute the nanosheets with the width of about 1.5 μm and thickness of 20 nm. The introduction of polymer (PVP) molecules and urea mainly contributes to the self-assembling process [29]. The porous Co_3O_4 nanoflower clusters could be yielded from the precursor (cobalt hydroxycarbonate) decomposition during the calcination process. Energy dispersive X-ray (EDX) spectrum (Fig. 3b) analysis clearly shows the existence of elemental Co and O, with an atomic ratio of Co to O in excess of 3:1. Based on the above analysis, it is clear that the Co_3O_4 nanoflower clusters structure could be formed when the precursors were calcined at 300 °C. The selected area diffraction pattern (SAED) pattern of the Co_3O_4 nanoflower clusters (Fig. 3c, inset) indicates that the material is of polycrystals nature, hence exposing various crystal planes at its surface [16].

The H_2-TPR profile of the catalyst in Fig. 4a shows two main reduction peaks at about 356 °C and 425 °C, which can be attributed to the reduction of Co_3O_4 into CoO and from CoO to metallic Co [30], respectively. The narrow peaks indicate the reduction process was fast. The curve also demonstrates Co^{3+} is reduced at first, and then the produced Co^{2+} and Co^{2+} in the catalyst itself are further reduced into metallic Co. The UV–vis spectrum of Co_3O_4 nanocrystals in Fig. 4b exhibits two absorption bands centered at 410 and 690 nm, which are assigned to the ligand-to-metal charge transfers of O^{II} to Co^{II} and O^{II} to Co^{III}, respectively [31]. Its optical band gap can be obtained by the following equation:

$$\alpha h\nu = A(h\nu - E_g)^n$$

α is the absorption coefficient, $h\nu$ is the photon energy, A is a constant relative to the material, E_g is the band gap, and n is either 2 for an indirect transition or 1/2 for a direct transition. The semiconductor of pure Co_3O_4 compound possesses direct transitions within the visible spectral region [31]. The $(ah\nu)^2 - h\nu$ curve for the products is shown in Fig. 4b inset, exhibiting two plots of linear relationship at 1.72 eV and 0.85 eV. The band gap of 1.72 eV should be associated with the $O^{2-} \rightarrow Co^{2+}$charge transfer process, while the band gap of 0.85 eV can be assigned to $O^{2-} \rightarrow Co^{3+}$ charge transfer. The multiple band gap energies (ΔE_g = 0.87 eV) for the Co_3O_4 nanostructure may also suggest the possibility of degeneracy of the valence band [32].

Because the Raman scattering is very sensitive to the microstructure of nanocrystalline materials, it is also used here to clarify the structure of the Co_3O_4 nanoflower clusters. As shown in Fig. 4c, the Raman spectrum of the Co_3O_4 nanoflower clusters shows four Raman peaks located at around 194, 475, 519 and 680 cm^{-1}, respectively corresponding to F_{2g}, E_g, F_{2g}, and F_{2g} phonon mode. All the shifts are consistent with those of pure crystalline Co_3O_4. In this test, the lattice vibration peaks of Co^{2+} and Co^{3+} cations are weak, broad and not fully displayed (the peak around 617 cm^{-1} corresponding to F_{2g} failed to appear).

The EPR spectrum of the sample Co_3O_4 is displayed in Fig. 4d. A highly symmetrical broad signal between maximum and minimum (ΔH_{pp} = 1150 G) is observed in the field region, which is stable only at low temperatures. The EPR parameters are $g_{xx} = g_{yy} = g_{zz} = g = 2.256$ by calculation, which may be assigned to unsaturated coordinated Co^{3+} – adsorbed O_2^- [33] in solid sample. This result proves that the unsaturated coordinated Co^{3+} – adsorbed O_2^- is more active at the surface of the as-prepared Co_3O_4 nanomaterials, and adsorbed O_2^- contributed to the catalytic oxidation reaction.

XPS is a reliable method for investigating the oxidation state of atoms in the top few layers of material surfaces with partially filled valence bonds. Fig. 5 presents the Co 2p XPS spectrum of the composite, which exhibits two peaks at 796.1 and 780.9 eV, corresponding to the Co $2p_{1/2}$ and Co $2p_{3/2}$ spin-orbit peaks of Co_3O_4, respectively. The shake-up satellites with a low intensity at ca. 8.7 eV from the main Co $2p_{3/2}$ spin orbit components are also characteristic of those of pure Co_3O_4 [34]. The presence of Co_3O_4 can be further confirmed by the O 1s XPS peak at 530.4 eV, which corresponds to the lattice oxygen in the Co_3O_4 phase. The small O 1s peak at 531.7 eV in the spectrum indicates the presence of surface-adsorbed oxygen such as O_2^{2-} or O^-, belonging to defect-oxide or hydroxyl-like group [35,36]. The presence of surface hydroxyl-like groups may result from oxygen vacancy on the surface of the Co_3O_4 sample originating from the dissociative adsorption of H_2O molecules. The oxide defects can adsorb and activate gaseous O_2 to form active oxygen species, which is beneficial to promote the oxidation reaction. The surface chemisorbed oxygen was reported to be highly active in oxidation reaction due to its higher mobility than lattice oxygen [36], and the high relative concentration ratio (2.25) of $O_{adsorbed}/O_{lattice}$ on catalyst surface could be correlated with high catalytic oxidation activity [37].

3.2. The catalytic activity of Co_3O_4 nanostructure

In order to investigate the catalytic activity of as-prepared Co_3O_4 nanoflower clusters towards toluene, we also fabricated Co_3O_4

blocks calcined at 400 °C and 500 °C (named Co-T_1, Co-T_2, Co-T_3, respectively) for comparison. The SEM images in the inset of Fig. 6a suggest these Co_3O_4 materials are no longer nanoflowers but in larger blocks with increasing the calcination temperature. The curves in Fig. 6a show the conversion of toluene as a function of the reaction temperature over the as-prepared catalysts. With increasing the calcination temperature, the catalytic activity of the catalysts is found to decline. The sections between 125 °C and 220 °C for all the three curves confirm that the conversion rates of toluene over the three samples are all low and less than 40%. Comparing the catalytic activity at 100% conversion, the following order of activities is established: Co-T_1 > Co-T_2 > Co-T_3. Although the crystallinity of the catalyst improved with increasing the calcination temperature, the specific surface areas of the catalysts are reduced at the same time (see Table 1), which causes the decline in the number of active sites on the surface of the catalysts. Moreover, low calcination temperature may benefit the reduction of surface oxygen, and then improve the reducibility of the catalyst [38]. However, surface area is not the only factor for determining the activity of the catalyst. Shen et al. [8] has proved that Co^{3+} cation was the active site in oxidation of CO from angle of crystal planes. The CO molecule interacted preferably with the surface Co^{3+} cation, which was the only favorable site for CO adsorption. In our work, the results of the EPR suggest the active site Co^{3+} is more dominant on the surface of the Co_3O_4 nanoflower clusters. We guess Co^{3+} cation may play an important role in the adsorption of toluene.

Table 1
Physico-chemical properties of the studied samples at different calcination temperatures.

Catalyst	S_{BET} (m^2/g)	Pore volume [a] (cm^3/g)	Average pore diameter [a] (nm)
Co_3O_4-T_1	62.08	0.1872	7.827
Co_3O_4-T_2	20.98	0.1994	2.192
Co_3O_4-T_3	17.45	0.1107	17.33

[a] Pore diameter and pore volume calculated by BJH method (desorption branch).

We further studied the stability of Co-T_1. The curve in Fig. 6 suggests that the toluene conversion rate of the Co_3O_4 nanoflower

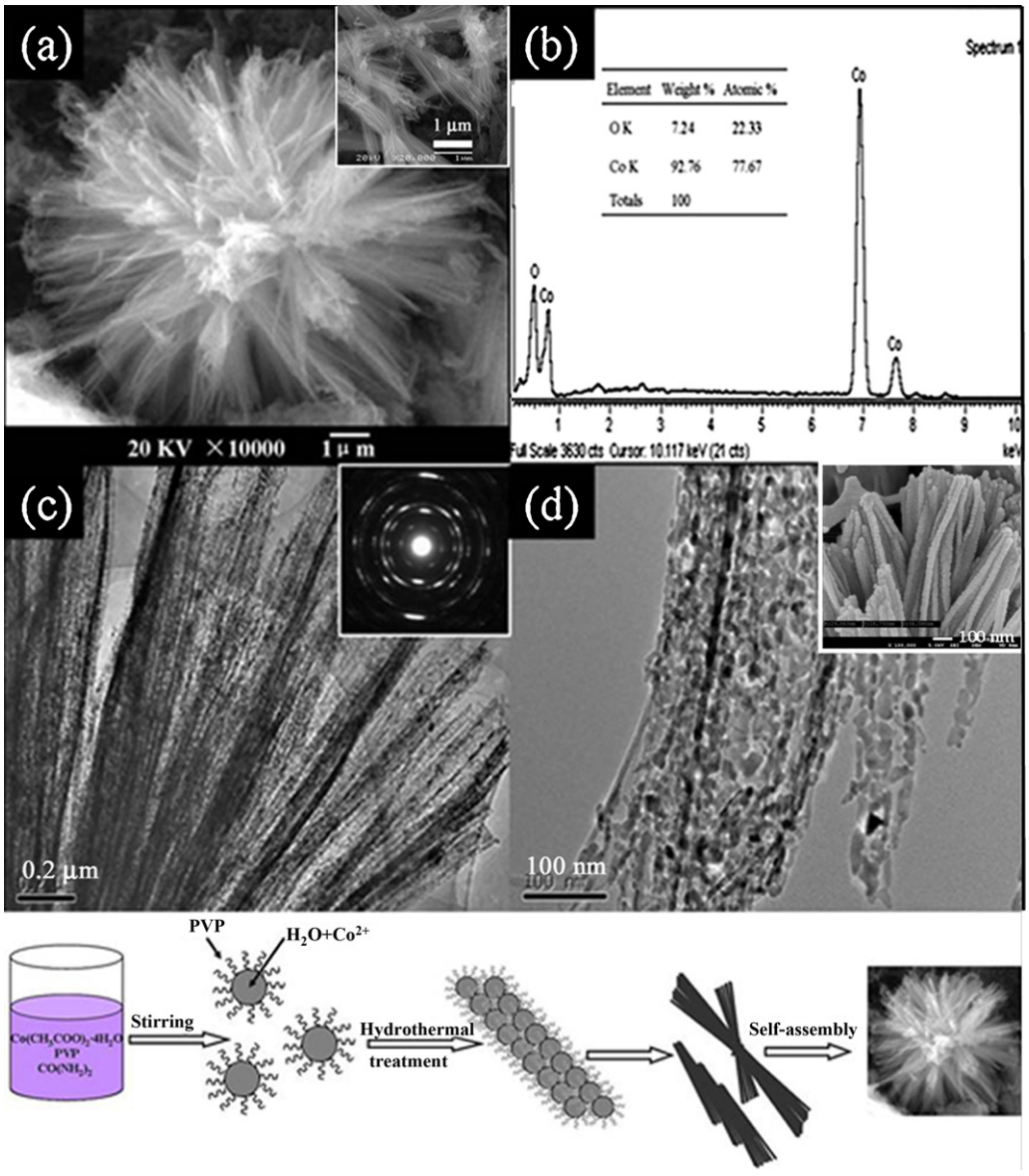

Fig. 3. (a) SEM image, (b) EDX spectrum, (c and d) TEM and SAED images of the as-prepared Co_3O_4 sample.

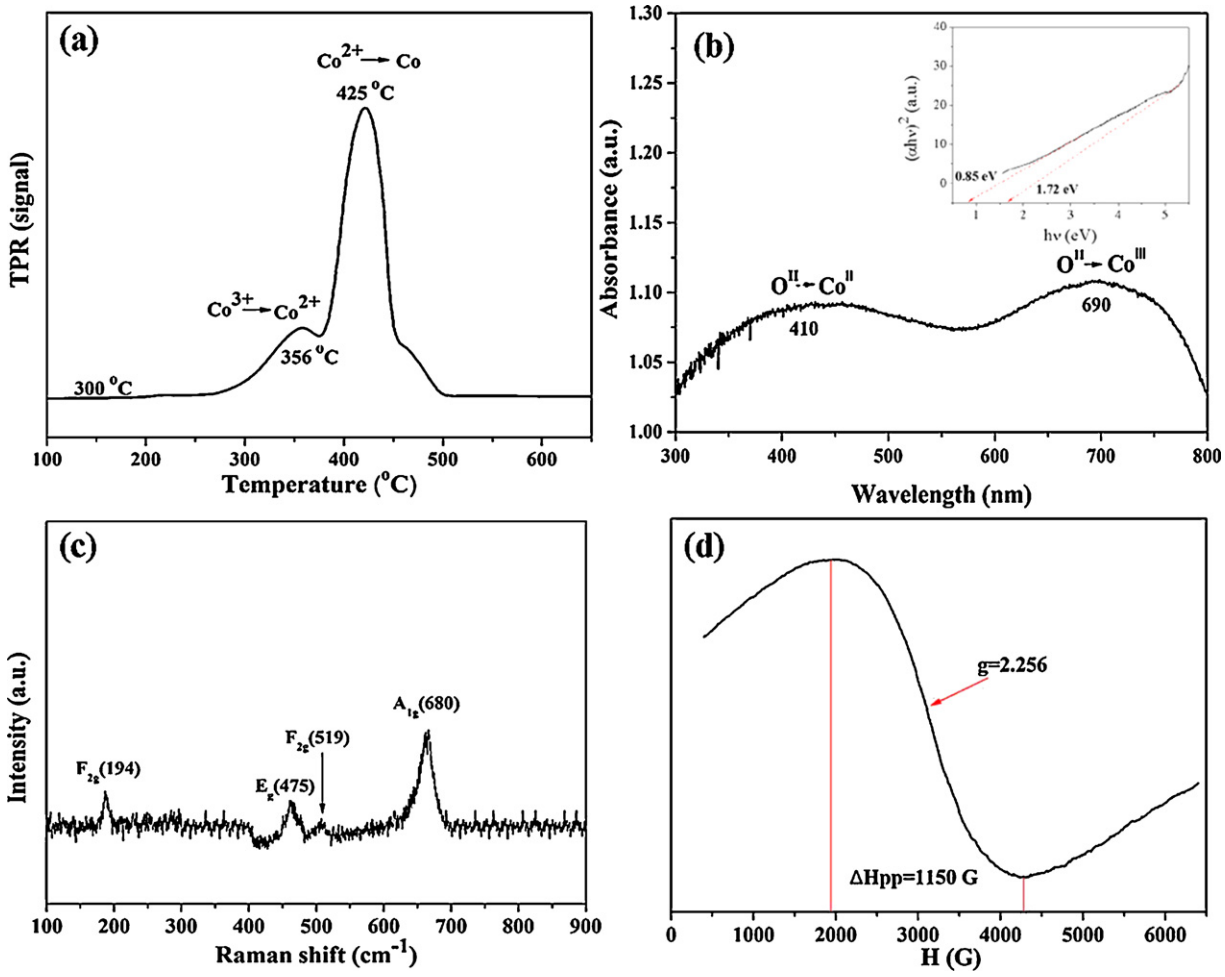

Fig. 4. (a) H_2-TPR profile of the as-prepared Co_3O_4 nanoflower clusters, (b) The UV–vis spectra and optical band gap energy of Co_3O_4 nanoflower clusters, (c) Raman spectrum of the as-prepared Co_3O_4 nanoflower clusters, (d) EPR pattern of the as-prepared Co_3O_4 nanoflower clusters.

clusters as catalyst was still above 90% after the reaction running for 50 h at complete conversion temperature (250 °C). Then the reactor space velocity was changed to 50,000 h^{-1} and 80,000 h^{-1}, respectively. The conversion and the life time experiments were re-operated under the new operation conditions. The curves D and E in Figs. 6a show the toluene activity of Co_3O_4 nanoflower clusters catalyst under different GHSV. Obviously, with GHSV from 37,500 h^{-1} to 50,000 h^{-1}, the toluene conversion curve slightly shifted to high temperature and 100% toluene conversion could still be achieved in a wide temperature range from 125 to 300 °C. However, the conversion rate of toluene obviously shifted to high temperature under a rather high GHSV of 80,000 h^{-1}, which is due to that the reactant gases may have less time to adsorb and react with the catalyst, thus leading to lower conversion. The curves B and C in Fig. 6b indicate that the toluene conversion rate of the Co_3O_4 nanoflower clusters as catalyst is also up to 90% after the reaction running for over 50 h under different space velocity, which suggests that the catalytic activity of the Co_3O_4 nanoflower clusters is fairly stable.

Therefore, it is indicated that the as-obtained Co_3O_4 nanoflower clusters calcined at 300 °C have the better activity for toluene oxidation with favorable stability. It is suggested that the calcination temperature strongly influences the morphology of the catalysts, and further affects their surface chemical properties.

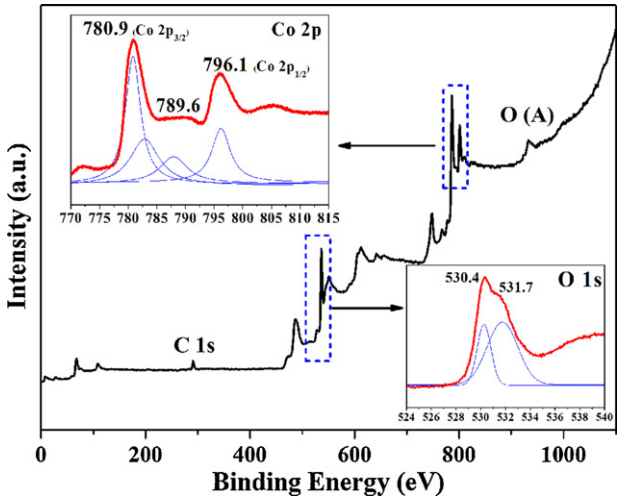

Fig. 5. XPS spectrum of the as-prepared Co_3O_4 nanoflower clusters, and Co 2p, O 1s Xp spectra obtained on the as-prepared Co_3O_4 nanoflower clusters.

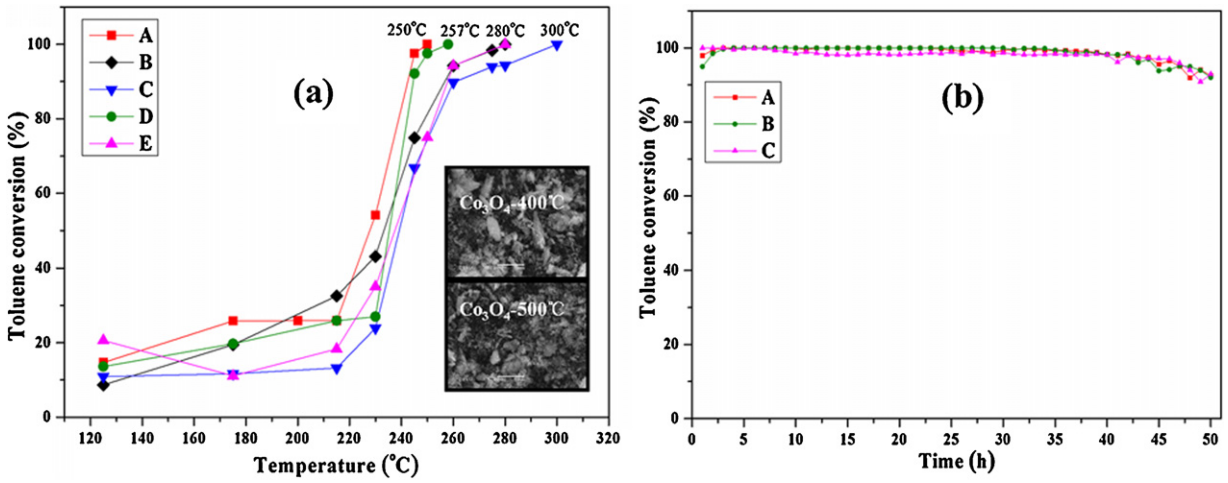

Fig. 6. (a) The conversion curves of toluene over the different as-prepared catalysts under different operation conditions: (A) Co_3O_4-T_1, GHSV = 37,500 h^{-1}; (B) Co_3O_4-T_2, GHSV = 37,500 h^{-1}; (C) Co_3O_4-T_3, GHSV = 37,500 h^{-1}; (D) Co_3O_4-T_1, GHSV = 50,000 h^{-1}; (E) Co_3O_4-T_1, GHSV = 80,000 h^{-1}. (b) Time dependence of toluene conversion: (A) Co_3O_4-T_1, GHSV = 37,500 h^{-1}, reaction temperature: 250 °C; (B) Co_3O_4-T_1, GHSV = 50,000 h^{-1}, reaction temperature: 257 °C; (C) Co_3O_4-T_1, GHSV = 80,000 h^{-1}, reaction temperature: 280 °C.

4. Conclusions

In this paper, we have obtained Co_3O_4 precursor by a low-temperature hydrothermal method. The products of Co_3O_4 flower-shaped nanoclusters were assembled by nanosheets composed of nanowires, which consisted of smaller nanoparticles with uniform size. The addition of PVP contributed to the formation of the unique morphology of Co_3O_4 nanoclusters with excellent stability. The synthetic approach of the model catalysts by two-step self-assembly reported here may also be extended to the synthesis of other functional nanomaterials.

The high relative concentration surface-adsorbed oxygen on the Co_3O_4 nanoflowers surface is highly active in oxidation of toluene due to its higher mobility than lattice oxygen. In addition, the oxide defects can adsorb and activate gaseous O_2 to form active oxygen species, which is beneficial to promote the toluene oxidation reaction. Comparing the catalysts with different morphologies in the catalytic oxidation of toluene, the Co_3O_4 nanoflowers exposed abundant Co^{3+} cations on the surface have a higher toluene conversion rate and good stability, which is also suggested that Co^{3+} cation may play an important role in the adsorption of toluene. In addition, the catalytic activity of the Co_3O_4 nanoflower clusters seriously affects by high GHSV, but is resistant to the long life time. The obtained Co_3O_4 nanomaterial is an attractive substitute for the noble metal catalysts.

Acknowledgments

This work was supported financially by the National Nature Science Foundation of China (NSFC-RGC 21061160495, 20837001), the National High Technology Research and Development Program of China (863 Program) (No. 2010AA064902), and the Excellent Talents Program of Liaoning Provincial University (LR2010090).

References

[1] K. Everaert, J. Degreve, J. Baeyens, VOC–air separations using gas membranes, J. Chem. Technol. Biotechnol. 78 (2003) 294–297.
[2] K. Everaert, J. Baeyens, Catalytic combustion of volatile organic compounds, J. Hazard. Mater. B 109 (2004) 113–139.
[3] X.F. Tang, J.H. Li, J.M. Hao, Synthesis and characterization of spinel Co_3O_4 octahedra enclosed by the {1 1 1} facets, Mater. Res. Bull. 43 (2008) 2912–2918.
[4] M.S. Wang, L.K. Zeng, Q.W. Chen, Controlled synthesis of Co_3O_4 nanocubes under external magnetic field and their magnetic properties, Dalton Trans. 40 (2011) 597–601.
[5] X.D. Lou, J. Han, W.F. Chu, X.F. Wang, Q.T. Cheng, Synthesis and photocatalytic property of Co_3O_4 nanorods, Mater. Sci. Eng. B 137 (2007) 268–271.
[6] F.F. Tao, C.L. Gao, Z.H. Wen, Q. Wang, J.H. Li, Z. Xu, Cobalt oxide hollow microspheres with micro- and nano-scale composite structure: fabrication and electrochemical performance, J. Solid State Chem. 182 (2009) 1055–1060.
[7] A.M. Cao, J.S. Hu, H.P. Liang, W.G. Song, L.J. Wan, X.L. He, X.G. Gao, S.H. Xia, Hierarchically structured cobalt oxide (Co_3O_4): the morphology control and its potential in sensors, J. Phys. Chem. B 110 (2006) 15858–15863.
[8] X.W. Xie, Y. Li, Z.Q. Liu, M. Haruta, W.J. Shen, Low-temperature oxidation of CO catalysed by Co_3O_4 nanorods, Nature 458 (2009) 746–749.
[9] F. Teng, W.Q. Yao, Y.F. Zheng, Y.T. Ma, T.G. Xu, G.Z. Gao, S.H. Liang, Y. Teng, Y.F. Zhu, Facile synthesis of hollow Co_3O_4 microspheres and its use as a rapid responsive CL sensor of combustible gases, Talanta 76 (2008) 1058–1064.
[10] Y.C. Chen, Y.G. Zhang, S.Q. Fu, Synthesis and characterization of Co_3O_4 hollow spheres, Mater. Lett. 61 (2007) 701–705.
[11] B.Y. Geng, F.M. Zhan, C.H. Fang, N. Yu, A facile coordination compound precursor route to controlled synthesis of Co_3O_4 nanostructures and their room-temperature gas sensing properties, Mater. Chem. 18 (2008) 4977–4984.
[12] X. Wang, L.J. Yu, X.L. Wu, F.L. Yuan, Y.G. Guo, Y. Ma, J.N. Yao, Synthesis of single-crystalline Co_3O_4 octahedral cages with tunable surface aperture and their lithium storage properties, J. Phys. Chem. C 113 (2009) 15553–15558.
[13] Z.G. Guo, W.M. Liu, Superhydrophobic spiral Co_3O_4 nanorod arrays, Appl. Phys. Lett. 90 (2007) 1–3.
[14] R. Xu, H.C. Zeng, Dimensional control of cobalt-hydroxide-carbonate nanorods and their thermal conversion to one-dimensional arrays of Co_3O_4 nanoparticles, J. Phys. Chem. B 107 (2003) 12643–12649.
[15] J. Yang, H.W. Liu, W.N. Martens, R.L. Frost, Synthesis and characterization of cobalt hydroxide, cobalt oxyhydroxide, and cobalt oxide nanodiscs, J. Phys. Chem. C 114 (2010) 111–119.
[16] H.Y. Liang, J.M. Raitano, L.H. Zhang, S.-W. Chan, Controlled synthesis of Co_3O_4 nanopolyhedrons and nanosheets at low temperature, Chem. Commun. (2009) 7569–7571.
[17] X. Wang, X.-L. Wu, Y.-G. Guo, Y.T. Zhong, X.Q. Cao, Y. Ma, J.N. Yao, Synthesis and lithium storage properties of Co_3O_4 nanosheet-assembled multishelled hollow spheres, Adv. Funct. Mater. 20 (2010) 1680–1686.
[18] L. Li, Y. Li, S.Y. Gao, N. Koshizaki, Ordered Co_3O_4 hierarchical nanorod arrays: tunable superhydrophilicity without UV irradiation and transition to superhydrophobicity, Mater. Chem. 19 (2009) 8366–8371.
[19] J. Liu, D.F. Xu, Hollow nanostructured anode materials for Li-ion batteries, Nanoscale Res. Lett. 5 (2010) 1525–1534.
[20] L.H. Hu, Q. Peng, Y.D. Li, Selective synthesis of Co_3O_4 nanocrystal with different shape and crystal plane effect on catalytic property for methane combustion, J. Am. Chem. Soc. 130 (2008) 16136–16137.
[21] T. Zhu, J.S. Chen, X.W. Lou, Shape-controlled synthesis of porous Co_3O_4 nanostructures for application in supercapacitors, J. Mater. Chem. 20 (2010) 7015–7020.
[22] V.R. Choudhary, G.M. Deshmukh, S.G. Pataskar, Low temperature complete combustion of dilute toluene and methyl ethyl ketone over transition metal-doped ZrO (cubic) catalysts, Catal. Commun. 5 (2004) 115–119.
[23] Z. Özcelik, G.P. Soylu, I. Boz, Catalytic combustion of toluene over Mn, Fe and Co-exchanged clinoptilolite support, Chem. Eng. J. 155 (2009) 94–100.
[24] C.Y. Lu, M. Wey, L. Chen, Application of polyol process to prepare AC-supported nanocatalyst for VOC oxidation, Appl. Catal: A Gen. 325 (2007) 163–174.
[25] A. Szegedi, M. Popova, C. Minchev, Catalytic activity of Co/MCM-41 and Co/SBA-15 materials in toluene oxidation, J. Mater. Sci. 44 (2009) 6710–6716.

[26] K. Jiraĭtovaĭ, J. Mikulovaĭ, J. Klempa, T. Grygar, Z. Bastl, F. Kovanda d., Modification of Co–Mn–Al mixed oxide with potassium and its effect on deep oxidation of VOC, Appl. Catal. A: Gen 361 (2009) 106–116.
[27] X.W. Xie, P.J. Shang, Z.Q. Liu, Y. Lv, Y. Li, W.J. Shen, Synthesis of nanorod-shaped cobalt hydroxycarbonate and oxide with the mediation of ethylene glycol, J. Phys. Chem. C 114 (2010) 2116–2123.
[28] H. Zhang, J.B. Wu, C.X. Zhai, X.Y. Ma, N. Du, J.P. Tu, D.R. Yang, From cobalt nitrate carbonate hydroxide hydrate nanowires to porous Co_3O_4 nanorods for high performance lithium-ion battery electrodes, Nanotechnology 19 (2008) 035711.
[29] Y.Z. Shao, J. Sun, L. Gao, Hydrothermal synthesis of hierarchical nanocolumns of cobalt hydroxide and cobalt oxide, J. Phys. Chem. C 113 (2009) 6566–6572.
[30] X.W. Xie, W.J. Shen, Morphology control of cobalt oxide nanocrystals for promoting their catalytic performance, Nanoscale 1 (2009) 50–60.
[31] Y.G. Zhang, Y.C. Chen, T. Wang, J.H. Zhou, Y.G. Zhao, Synthesis and magnetic properties of nanoporous Co_3O_4 nanoflowers, Micropor. Mesopor. Mater. 114 (2008) 257–261.
[32] R. Xu, H.C. Zeng, Self-generation of tiered surfactant superstructures for one-pot synthesis of Co_3O_4 nanocubes and their close- and non-close-packed organizations, Langmuir 20 (2004) 9780–9790.
[33] C.A. Querini, M.A. Ulla, F. Requejob, J. Soria, U.A. Sedrh, E.E. Mirba, Catalytic combustion of diesel soot particles. Activity and characterization of Co/MgO and Co, K/MgO catalysts, Appl. Catal. B: Environ. 15 (1998) 5–19.
[34] T. He, D.R. Chen, X.L. Jiao, Y.L. Wang, Y.Z. Duan, Solubility-controlled synthesis of high-quality Co_3O_4 nanocrystals, Chem. Mater. 17 (2005) 4023–4030.
[35] M. Kang, E.D. Park, J.M. Kim, J.E. Yie, Manganese oxide catalysts for NO_x reduction with NH_3 at low temperatures, Appl. Catal. A: Gen. 327 (2007) 261–269.
[36] Z. Wu, R. Jin, Y. Liu, H. Wang, Ceria modified MnO_x/TiO_2 as a superior catalyst for NO reduction with NH3 at low-temperature, Catal. Commun. 9 (2008) 2217–2220.
[37] F.D Liu, H. He, Y. Ding, C.B. Zhang, Effect of manganese substitution on the structure and activity of iron titanate catalyst for the selective catalytic reduction of NO with NH_3, Appl. Catal. B: Environ. 93 (2009) 194–204.
[38] K.-J. Kim, H.-G. Ahn, Complete oxidation of toluene over bimetallic Pt–Au catalysts supported on ZnO/Al_2O_3, Appl. Catal. B: Environ. 91 (2009) 308–318.